BIOCHEMICAL KINETICS MODEL OF DSB REPAIR AND γH2AX FOCI BY NON-HOMOLOGOUS END JOINING

Francis A. Cucinotta[1,*], Janice M. Pluth[2], Jennifer A. Anderson[3],

Jane V. Harper[3], and Peter O'Neill[3]

[1]*NASA, Lyndon B. Johnson Space Center, 2101 NASA Parkway, Houston TX 77058, USA*

[2]*Lawrence Berkeley National Laboratory, Life Sciences Division, One Cyclotron Road, Building 74, Berkeley, CA 94720, USA*

[3]*DNA Damage Group, Radiation and Genome Stability Unit, Medical Research Council, Harwell, Didcot, Oxfordshire, OX11 0RD, UK*

*****Corresponding author
Francis A. Cucinotta
Phone: 281-484-0968
Fax: 281-483-3058
E-mail: Francis.A.Cucinotta@nasa.gov

20 Pages of text,
1 Table
7 Figures,
1 Page of figure legends.

KEYWORDS: DNA damage repair, Non-homologous end-joining, γH2AX foci, systems biology, mathematical models

RUNNING TITLE: Biochemical Kinetics Model of DSB Repair by NHEJ

BIOCHEMICAL KINETICS MODEL OF DSB REPAIR AND γH2AX FOCI BY NON-HOMOLOGOUS END JOINING

Francis A. Cucinotta[1], Janice M. Pluth[2], Jane V. Harper[3], and Peter O'Neill[3]

ABSTRACT:

We developed a biochemical kinetics approach to describe the repair of double strand breaks (DSB) produced by low LET radiation by modeling molecular events associated with the mechanisms of non-homologous end-joining (NHEJ). A system of coupled non-linear ordinary differential equations describes the induction of DSB and activation pathways for major NHEJ components including $Ku_{70/80}$, DNA-PKcs, and the Ligase IV-XRCC4 hetero-dimer. The autophosphorylation of DNA-PKcs and subsequent induction of γH2AX foci observed after ionizing radiation exposure were modeled. A two-step model of DNA-PK_{cs} regulation of repair was developed with the initial step allowing access of other NHEJ components to breaks, and a second step limiting access to Ligase IV-XRCC4. Our model assumes that the transition from the first to second-step depends on DSB complexity, with a much slower-rate for complex DSB. The model faithfully reproduced several experimental data sets, including DSB rejoining as measured by pulsed-field electrophoresis (PFGE), quantification of the induction of γH2AX foci, and live cell imaging of the induction of $Ku_{70/80}$. Predictions are made for the behaviors of NHEJ components at low doses and dose-rates, where a steady-state is found at dose-rates of 0.1 Gy/hr or lower.

INTRODUCTION

A mechanistic description of the processing of DNA double strand breaks (DSB) is important for the understanding of ionizing radiation effects leading to cell death, mutation, genomic instability, and carcinogenesis. Mathematical models of DSB repair are important for the description of radiation modalities not accessible by experimental means and for their possible predictive capabilities. Past mathematical models of ionizing radiation induced DSB repair have largely relied on phenemological approaches, which did not consider specific molecular interactions involved in DSB repair (1-3). Previously, we had shown that a biochemical approach based on non-linear kinetics enjoys some special features in describing DSB repair, including the time delay caused by a DSB-repair enzyme intermediate complex (3). Application of biochemical kinetics models to describe molecular DSB repair experimental data is a goal of the present study.

Non-homologous end joining (NHEJ) is the primary pathway for DSB repair in eukaryotic cells (4-6), and defects in NHEJ increase radiation sensitivity and the risk of carcinogenesis (7, 8). Many of the steps involved in NHEJ have been characterized experimentally, including the initial recognition of DSB's by the $Ku_{70/80}$ heterodimer, subsequent recruitment of the DNA dependent protein kinase catalytic subunit (DNA-PK_{cs}), and formation of the DNA dependent protein kinase (DNA-PK) (6-9). DNA-PK_{cs} contains several serine-threonine residues which are auto-phosphorylated. Auto-phosphorylation of various subsets of these sites is thought to be important in regulating pathway choices between NHEJ or homologous recombination repair (HR) (6). In

addition to DNA-PK_{cs}, a number of other proteins have been implicated as being important in either NHEJ or HR. For example, Artemis in conjunction with both ATM and DNA-PK_{cs} has been suggested to function in DNA end-processing of specific, difficult to repair, IR-induced damages (10-13), and both Ligase IV and XRCC4 have been shown to be important in the ligation step of NHEJ (14, 15).

DNA-PK_{cs} is a member of the phosphoinositide-3-kinase-realted protein kinase (PIKK) family, which includes ataxia-telangiectasia mutated (ATM), and ataxia-telangiectasia and Rad3-related (ATR) proteins, and these proteins play a role in sensing DNA damage (5). In addition to damage sensing, both ATM and ATR have been shown to have distinct roles from DNA-PKcs, consisting of G1/S, S and G2/M cell cycle checkpoints regulation (5, 16) and replication stress response (19), respectively. DNA-PKcs, ATM, and ATR share common features including a conserved carboxy-terminal motif (5), and a reliance on upstream activators, $Ku_{70/80}$, the MRE-Rad50-Nbs1 complex (MRN), and ATRIP, respectively. ATR is believed to function largely in S-phase, whereas DNA-PK_{cs} and ATM have important roles throughout the cell cycle (16-19). The activation step of DNA-PK_{cs} and ATM is rapid occurring from a few to about 30-minutes as observed in recent studies (5, 9, 18). Both activated proteins have been shown to lead to the phosphorylation of the histone variant H2AX in a chromatin region corresponding to about 2-Mbp around the DSB, with the phosphorylated form denoted γH2AX (20, 21). Total numbers of γH2AX foci have been shown to be fairly representative of the total number of DSB (20, 22, 23). In addition, a correlation between γH2AX foci loss and radiation sensitivity has been noted (23-25).

The plethora of experimental studies involving NHEJ repair should facilitate the development of mathematical models of these processes. In this paper we have developed a systems biology approach to NHEJ repair that can be used to make predictions for other radiation modalities, including extrapolations to low doses and dose-rates. Systems biology seeks to describe emergent properties of biological systems from the interactions of molecules acting in specific pathways (26). We use this approach to describe DSB rejoining curves, and the kinetics of formation and loss of γH2AX to gain insights into the kinetics of NHEJ repair pathway. A key component of a biochemical kinetics model is the role of DNA repair complex intermediates, which leads naturally to a non-linear kinetics description (3). We consider several intermediate complexes based on γH2AX radiation induced repair foci (RIRF) data, and DNA-PK_{cs} experimental studies, and relate their description to pulsed-field gel electrophoresis (PFGE) DSB rejoining curves.

Ionizing radiation produces DSBs that vary from simple to complex structures and are produced with equal proportions with increasing dose, and depend on radiation quality (27, 28). Clustered DNA damage sites are defined as two or more elemental lesions within one or two helical turns of DNA produces by a single radiation track (27, 29). Under this definition all DSB are clustered damages, however complex DBS's are defined by the addition of other damage type such as base-damage, damaged ends, single-strand breaks near a DSB, or for two or more DSB in close proximity. Clustered non-DSB's can lead to secondary DSB's produced during damage processing (29, 30). For low LET radiation it has been estimated that 20-40% of the initial damage is complex

(27-29). Closely space multiple DSB could inhibit the attachment of repair proteins to other nearby DSB, and this possibility increases with the ionization power or linear energy transfer (LET) of radiation. We hypothesize that damage processing of complex DSB involve additional NHEJ factors including Artemis (10-13), MRN (19) and ATM proteins (10).

METHODS

DNA-PK Regulation and Repair Complexes

We use the mass-action chemical kinetics approach to describe the binding of repair enzymes to DSB's with several intermediate repair complexes leading to DNA rejoining: 1) an initial complex bound by the $Ku_{70/80}$ hetero-dimer, 2) Ku mediated DNA-PK_{cs} binding, 3) The regulation of the DSB-DNA-PK_{cs} complex through auto-phosphorylation by DNA-PK, and 4) a final repair complex involving the Ligase IV/XRCC4 heterodimer, denoted *LiIV*. **Figure 1** shows a schematic diagram of our model showing the sequence of proteins binding to the repair complex and the two activation steps considered; phosphorylation of DNA-PK_{cs} and H2AX. The series of repair complexes are denoted C_j or with super-scripts P for auto-phosphorylation in complex, for e.g. C_j^P. The first complex (C_1) is formed by $Ku_{70/80}$ binding to the DSB, and the second binding by DNA-PK_{cs} to the first complex forming C_2 etc., through to the final ligation step. Because these proteins are post-transcriptionally regulated the total number of enzymes in free-form or complex form is assumed to be conserved.

DSB are assumed to be induced per unit dose-rate with efficiency, α (Gy^{-1} per cell). The $Ku_{70/80}$ hetero-dimer is highly abundant and rapidly attaches to the DSB (denoted as C_0) leading to the mass-action equation

$$(1) \quad \frac{d[C_0]}{dt} = \alpha \frac{dD}{dt} - k_1[Ku_{70/80}][C_0]$$

forming the repair complex, C_1, which is followed quickly by DNA-PK_{cs} binding

$$(2) \quad \frac{d[C_1]}{dt} = k_1[C_0][Ku_{70/80}] - k_2[DNAPK_{cs}][C_1]$$

to form a second complex, C_2. Equations (1) and (2) follow the convention that symbols within brackets define for a given molecular species, the time-dependent number of copies per cell. The repair complex, C_2, is then modified by phosphorylation events that facilitate cleaning of the ends, signal transduction, and the translation of DNA-PK_{cs} away from the ends of the break to allow ligation by LigaseIV/XRCC4 complex. Auto-phosphorylation of a cluster of residues on DNA-PK_{cs}, denoted ABCDE, is expected to be a gate-keeper regulating access to the break by other repair proteins (6). The phosphorylation of a second cluster of residues on DNA-PK_{cs}, denoted PQR, has been suggested to promote HR (6), whereas phosphorylation of the ABCDE cluster is thought to inhibit HR (6). The PQR cluster has been noted to partially facilitate dissociation of DNA-PK from the ends, however it is expected that other phosphorylation sites are needed for complete disassembly (6). To date, phosphorylation of $Ku_{70/80}$ has not been

implicated as being critical for the actual repair of DSB (31) shown and thus will not be considered in the model.

We consider a two-step model that depicts DNA-PK_{cs} role in regulation of repair involving activation events controlled by auto-phosphorylation of DNA-PK_{cs}. The exact nature of the auto-phosphorylation of DNA-PK_{cs} is not known (6, 32, 33), autophosphorylation may occur in *trans,* where one DNA-PK_{cs} molecule phosphorylates a second molecule on opposing sides of a DSB; a second-order reaction. Alternatively, it may occur in *cis*, by an intra-molecular mechanism; a first-order reaction. Both of these mechanisms may occur and could depend on the DSB end structure (32, 33).We have modeled the auto-phosphorylation of DNA-PK_{cs} bound to the DSB ends as first-order for both steps in DNA-PK_{cs} regulation of repair. We assume the second-step depends on the complexity of the DSB and may involve other proteins, including Artemis and other poorly defined repair proteins. Residual breaks are predicted at complex DSB sites through a competing first-order process that assumes not all complex DSB are successfully rejoined with the failure occurring before the transition to the ligation step of the reaction. The resulting equations are

$$(3)\quad \frac{d[C_2]}{dt} = k_2[DNAPK_{cs}][C_1] - k_{P_1}[C_2]$$

$$(4)\quad \frac{d[C_2^{\,P}]}{dt} = k_{P_1}[C_2] - k_{P_2}[C_2^{\,P}] - k_{res}[C_2^{\,P}]$$

$$(5)\quad \frac{d[C_2^{PP}]}{dt} = k_{P_2}[C_2^{P}] - k_3[LiIV][C_2^{PP}]$$

$$(6)\quad \frac{d[DSB_{res}]}{dt} = k_{res}[C_2^{P}]$$

The rates, k_{P2} and k_3 are assumed to depend on the complexity of the DSB, and k_{res} set to zero for simple DSB.

Finally, the last step in our model involves ligation of the ends by the Ligase IV/XRCC4 complex, denoted *LiIV*, and enzyme release given by

$$(7)\quad \frac{d[C_3]}{dt} = k_3[LiIV][C_2^{PP}] - k_{D_C}[C_3]$$

The Ligase IV/XRCC4 complex is also regulated by covalent modifications (13), but this observation is not currently treated in our model.

γH2AX Foci Kinetics

The histone variant H2AX is phosphorylated after DNA damage by each of the family of PIK3 phospho-proteins ATM, ATR, and DNA-PK_{cs} (5). In the G1 phase of the cell cycle, ATM and DNA-PK_{cs} phosphorylate H2AX with nearly equal efficiencies and in an overlapping manner (34). γH2AX foci appear at a distance from DSB corresponding to a region of 2 Mbp (20), and it is not known how many H2AX molecules are modified per

DSB or of the mechanism that leads to phosphorylation of a large number of H2AX molecules. We use Michaelis-Menten kinetics to describe the induction rate of H2AX by DNA-PKcs in its active forms as given by,

$$(8) \qquad \frac{d[\gamma H2AX]}{dt} = \frac{k_{P\gamma}[C_{DNA-PKcs}][H2AX]}{K_M + [C_{DNA-PKcs}]} - k_{D\gamma}[\gamma H2AX]$$

where $[C_{DNA\text{-}PKcs}]$ is the sum of active forms of DNA-PKcs (C_2^P, C_2^{PP}, and C_3). The mechanism of de-phosphorylation of γH2AX foci has not been well studied. We assume this step follows a simple first-order decay law in Eq. (8).

Scaling Variables

In order to simplify the model solutions, we introduce new scaled-variables by considering the conservation relations for the total concentration of a given protein, and noting the sum of all repair complexes is equal to the initial number of DSB. The new scaled variables are introduced using the definitions,

$$H_i = [E_i] + \sum_{j=i}^{n}[C_j] = const.; \quad h_i(t) = \frac{\sum_{j=i}^{n}[C_j]}{H_i}; \quad \kappa_i = H_i k_i$$

and

$$c_i(t) = \frac{[C_i]}{H_1}$$

which after substitution leads to the system of equations

(9) $$\frac{dc_0(t)}{dt} = \frac{\alpha}{H_1}\frac{dD}{dt} - \kappa_1 c_0(t)(1-h_1(t))$$

(10) $$\frac{dc_1(t)}{dt} = \kappa_1 c_0(t)(1-h_1(t)) - \kappa_2 c_1(t)(1-h_2(t))$$

(11) $$\frac{dc_2(t)}{dt} = \kappa_2 c_1(t)(1-h_2(t)) - k_{P_1} c_2(t)$$

(12) $$\frac{dc_2^{\,P}(t)}{dt} = k_{P_1} c_2(t) - (k_{P_2} + k_{res}) c_2^{\,P}(t)$$

(13) $$\frac{dc_2^{\,PP}(t)}{dt} = k_{P_2} c_2^{\,P}(t) - \kappa_3 c_2^{\,PP}(t)(1-h_3(t))$$

(14) $$\frac{dc_{res}(t)}{dt} = k_{res} c_2^{\,P}(t)$$

(15) $$\frac{dc_3(t)}{dt} = \kappa_3 c_2^{\,PP}(t)(1-h_3(t)) - k_{D_C} c_3(t)$$

All rate-constants are assumed to be independent of the type of initial DSB, except for k_{P2} and κ_3, which are given distinct values for simple and complex DSB, respectively. For the solutions in terms of the scaled-variables, only the value of H_1 enters as all other H_i are combined with the k_i to form the rate parameters, κ_i which are in units of Hr^{-1}. The

functions h_i(t) include contributions from repair complexes involving both simple and complex DSB's.

The histone variant, H2AX content varies with cell lineage representing from 2 to 10% of all nucleosomes and there are about 2.0 x10^6 H2AX molecules per cell (20). We reasoned that it was more useful to model the kinetics of the number of γH2AX foci formed, rather than the number of activated molecules. For foci counting experiments the number of foci is limited by the model dependent initial number of DSB per cell. For low LET radiation the probability of more than one DSB within the spatial region of foci is small, however for high LET other considerations will be needed to be taken into account (Cucinotta *et al.*, in preparation). Assuming [γH2AX]+[H2AX] = constant, and denoting γ(t) as the time dependent number of foci leads to

$$(16) \quad \frac{d\gamma(t)}{dt} = \frac{\kappa_{P_\gamma} c_{DNA-PKcs}(t)(1-\gamma(t))}{\kappa_M + c_{DNA-PKcs}(t)} - k_{D_\gamma}\gamma(t)$$

where $\kappa_{P\gamma} = k_{P\gamma} / H_1$. For comparison to DSB rejoining kinetics in an acute irradiation measured using PFGE, the number of DSB's remaining is given by

$$(17) \quad DSB_{remaining}(t) = H_1[\sum_{j=0}^{3} c_j(t) + c_{res}(t)]$$

For comparison to experimental data on relative $Ku_{70/80}$ induction, which includes $Ku_{70/80}$ in various DSB repair complexes the following sum is used

$$(18) \quad C_{Ku_{70/80}}(t) = H_1 \sum_{j=1}^{3} c_j(t)$$

The system of equations formulated above to represent NHEJ are non-linear ordinary differential equations, described as stiff equations describing equations were the values for the various parameters, k_i or κ_i vary over several orders of magnitude. These equations were solved numerically using the method of backward difference approximates. We note that the factors '*1-h_i*' in our scaled equation have values close to unity at low doses where the initial number of DSB is <<H_1.

RESULTS AND DISCUSSION

Our kinetics model of NHEJ consists of a system of 8 coupled non-linear ordinary differential equations for each class of DSB (simple and complex). This system of equations describe major components in the NHEJ repair pathway and the phosphorylation of H2AX by DNA-PK_{cs}. Values for rate-constant were determined by comparing to experimental data with cell lineage specific values estimated for rate-constants and other parameters are listed in **Table 1**. Our scaling approach results in a significant reduction in parameter space since it avoids the need to estimate values for the total cellular concentration of $Ku_{70/80}$, DNA-PK_{cs}, LiIV, and XRCC4, which are effectively replaced by a single constant, H_1. The value of H_1 can be interpreted as the total number of copies of $Ku_{70/80}$. However in the model other constants, H_j, could be used as the scaling variable, and we prefer to interpret the value of H_1 as the total

number of DNA-repair complexes that could occur in a cell (3). We have fixed this value at a large number (H_1=3000), to ensure that the shape of the DSB rejoining curve is largely independent of dose, over the range from 1 to 40 Gy. To reduce the number of variable parameters, we fixed the peak time of the $[C_1]$ complex, corresponding to the binding of $Ku_{70/80}$ to DSB, at about 1 min post-irradiation (35), and of the $[C_2]$ complex, corresponding to the binding of DNA-PK_{cs} complex, at about 3 min for all cell lineages considered using the values for κ_1 and κ_2 as listed in **Table 1**. In-vitro assays provide insights into rates for DNA-PKcs activation occurring over times up to 30 min under different conditions (32, 36, 37). The remaining parameters are determined in a cell-lineage specific manner by comparing the model solutions to data for DSB rejoining, and the induction and loss of γH2AX foci.

Figures 2 illustrates the model predictions for the time evolution for the sequence of repair complexes formed at an acute dose of 1 Gy for simple and complex damage processing. We compared the model prediction to recent results using live cell imaging of DSB induced by a near infrared laser (NIR) of $Ku_{70/80}$ (35) in **Figure 3**. Our result using eq. (18), which represents the sum over different repair complexes containing the $Ku_{70/80}$, is in excellent agreement with the live cell imaging observations where DSB's are induced by a near infrared laser (NIR) (35). There will be differences in the initial number and types of breaks, perhaps due to higher DSB induction by NIR as compared to that of X-rays at 1 Gy, however the agreement found over the first few hours of repair lends support to the values for the rate-constants chosen.

We also compared our model to the rejoining kinetics determined by PFGE, which is available in the literature for X-rays. DSB rejoining kinetics measured by PFGE are made at high dose (>10 Gy) and must be corrected for the presence of heat-labile sites (29, 38, 39), which account for up to 50% of the fragment yields at early post-irradiation times (within 30 mins post-irradiation). To avoid the contribution of heat-labile sites, we compared PFGE data analyzed using the cold lysis method developed by Rydberg (38) to the data of Sternerlow *et al*. (39) for the GM5758 diploid fibroblast cells as shown in **Figures 4.** We have used experimentally determined values from Gulston *et al.* (29) for HF19 cells for the value of α, the total number of DSB per Gy, of 25 and 16, respectively as initial conditions, and assume that 20% of the initial breaks repair with additional processing steps between the transition from C_2^P to C_2^{PP} and hence slower kinetic parameters. At moderate doses (<5 Gy) the model predicts a lack of rejoining in the first few minutes post-irradiation as the multiple steps in NHEJ proceed. However, there may be some DSB rejoined by direct ligation independent of DNA-PK_{cs} (35) leading to a faster component at early times, beyond those contributed by heat-labile sites.

Track structure calculations provide some estimates of the fraction of simple and complex DSB lesions. However, the bevy of mechanisms that would be available to repair the differential spectrum of DSB produced by ionizing radiation are not well understood and may utilize additional factors amongst these being Artemis (10-13), ATM (10), MRN (19, 40), Werner syndrome (41) proteins, and perhaps components in the nucleotide or base- excision repair pathways. In our model we assume just two average

components corresponding to so-called broad categories namely simple and complex DSB.

The fraction of residual breaks is easily modeled when the complex DSB are considered, if one assumes a first-order process results near the end of the cascade described above. We used a first-order rate-constant for residual break formation of 0.05 h^{-1} assuming a small fraction corresponding of the initial complex DSB are remain un-repaired at the C_2^P complex and lead to residual DSB. The model presented here thus provides a framework to describe the dependence of residual breaks on radiation quality, dose-rate, and post-irradiation time.

We compared our model to data for the time courses and dose-response for γH2AX foci. Leatherbarrow *et al.* (23) using confocal microscopy precisely measured the number of γH2AX foci in V79 and HF19 cells. We find good agreement with their results as shown in **Figure 5**. Comparisons of the number of γH2AX foci at 0.5 and 4 hr post-irradiation made by Short *et al*. (42) are shown in **Figure 6**. The model calculation shows a linear response at 0.5 hr post-irradiation. There is a concomitant induction of γH2AX from active ATM (34) monomers, which has not been studied in the current model. ATM and DNA-PK_{cs} are expected to induce these foci with nearly equal efficiency (34).

The understanding of dose-rate effects is an important consideration in radiation protection (43, 44). Since the processing of DSB after radiation is a determinant in mutation, chromosome aberrations, and carcinogenesis, we studied the induction of

various NHEJ components as a function of variable dose-rates and doses. Steady-state solutions for the systems equations can be found in closed form and compared with numerical solutions, and dose-rates where the steady-state, with foci counts independent of dose-rate, are obtained identified. The results of **Figure 7** predict that the number of DSB repair complexes per cell becomes independent of dose-rate below about 0.1 Gy/hr. These observations can be tested with experiments. Also, for model building our description of NHEJ can be used as a starting point for mechanistic models of mutation and chromosomal aberrations. In addition, studying dose-rate dependencies for repair should be informative in understanding dose-rate effects for these other endpoints.

In summary, we have synthesized a large number of experimental observations into a biochemical kinetics model of the NHEJ repair pathway. The model is based on the current mechanistic understanding of molecular binding and kinase activity of major NHEJ components that have been described experimentally and is capable of describing the time-courses, and dose and dose-rate dependencies for major NHEJ components, the induction of γH2AX foci upon activation of DNA-PK_{cs} through auto-phosphorylation, and DSB rejoining curves as measured by PFGE. The model presented here can be modified as understanding on molecular mechanisms of NHEJ repair is obtained. The ability to describe the kinetics of DSB induction and repair and the various associated protein complexes will support models of chromosomal aberrations as a function of radiation quality, when descriptions of DSB complexity and spatial dependence of initial DSB are coupled to the present model (27, 28, 45). We plan on extending our work to include theoretical descriptions of the fractions of simple and complex initial DSB for

high LET radiation, and the resulting changes in DSB repair and foci kinetics and to include the description of the ATM signaling pathway in our model.

ACKNOWLEDGMENTS

Support was provided by the US DOE (DE-FG02-05ER64090 and DE-A103-05ER64088) and NASA (03-OBPR-07-0032-0027).

REFERENCES

1. D.T. Goodhead, Saturable repair models of radiation action in mammalian cells, *Radiat. Res.*, **104**, S58-S67 (1985).

2. J. Kiefer, A repair fixation model based on classical enzyme kinetics. In Quantitative Models in Radiation Biology, ed. J. Kiefer, Springer-Verlag, Berlin, 171-180 (1988).

3. F.A. Cucinotta, H. Nikjoo, P. O'Neill, D.T. Goodhead, Kinetics of DSB rejoining and formation of simple chromosome exchange aberrations. *Int. J. Radiat. Biol*. **76**, 1463-1474 (2000).

4. S.P. Lees-Miller, and K. Meek, Repair of DNA double strand breaks by non-homologous end-joining. *Biochemie* **85**, 1161-1173 (2003).

5. J. Falck, J. Coates, and S.P. Jackson, Conserved modes of recruitment of ATM, ATR, and DNA-PK_{cs} to sites of DNA damage. *Nature* **434**, 605-611 (2005).

6. X. Cui, Y. Yu, S. Gupta, Y.M. Cho, S. Lees-Miller, and K. Meek, Autophosphorylation of DNA-dependent protein kinase regulates DNA end processing and may also alter double-strand break repair choice. *Mol. Cell Biol.* **25**, 10842-10652, 2005.

7. D.O. Ferguson, J.M. Sekiguchi, S. Chang, K.M. Frank, Y.Gao, R.A. DePinho, and F.W. Alt, The nonhomologous end-joining pathway of DNA repair is required for genomic instability and the suppression of translocations. *Proc. Natl. Acad. Sci.* USA **97**, 6630-6633 (2000).

8. M. Martin, A. Genesca, L. Lutre, I. Jaco, G.E. Taccioli, J. Egozcue, M.A. Blasco, G. Illiakis, and L. Tusell, Post-replicative joining of DNA double strand breaks causes genomic instability in DNA-PK_{cs}-deficient mouse embryonic fibroblasts. *Cancer Res.* **65**, 10223-10232 (2005).

9. D.W. Chan *et al.*, Autophosphorylation of the DNA-dependent protein kinase catalytic subunit is required for rejoining of DNA double strand breaks. *Genes Dev.* **16**, 2333-2338 (2002).

10. J. Drouet, P. Frit, C. Delteil, J.P. de Villartay, B. Salles, and P. Calsou, Interplay between Ku, Artemis, and the DNA-dependent protein kinase catalytic subunit at DNA ends**.** *J. Biol. Chem.* **281**, 27784 – 27793 (2006).

11. P. Jeggo, and P. O'Neill, The Greek Goddess, Artemis, reveals the secrets of her cleavage. *DNA Repair* **1**, 771-777 (2002).

12. J. Wang, J.M. Pluth, P.K. Cooper, M.J. Cowan, D.J. Chen, S.M. Yannone, Artemis phosphorylation and function in response to damage. *DNA Repair* **4**, 556-570 (2005).

13. E. Riballo, M. Kuhne, N. Rief, *et al.*, A pathway of double-strand break rejoining dependent upon ATM, Artemis and proteins locating to γ-H2AX foci. *Mol. Cell.* **16**, 715-724 (2004).

14. H. Wang, Z.C. Zeng, A.R. Perrault, X. Cheng, W. Qin, and G. Iliakis, Genetic evidence for the involvement of DNA Ligase IV in the DNA-PK-dependent pathway of non-homologous end joining in mammalian cells. *Nucl. Acids Res.* **29**, 1653-1660 (2001).

15. J. Drouet, C. Delteil, J. Lefrancois, P. Concannon, B. Salles, and P. Calsou, DNA-dependent protein kinase and XRCC4-DNA Ligase IV mobilization in the cell in response to DNA double strand breaks. *J. Biol. Chem.* **280**, 7060-7069 (2005).

16. K.D. Brown, Y. Ziv, S.N. Sadanandan, L. Chess, F.S. Collins, Y. Shiloh, and D.A. Tagle, The ataxia-telangiectasia gene product, a constitutively expressed nuclear protein that is not upregulated following genome damage. *Proc. Natl. Acad. Sci. USA* **94**, 1840-1845 (1997).

17. D.P. Gately, J.C. Hittle, G.K.T. Chan, and T.J. Yen, Characterization of ATM expression, localization, and associated DNA-dependent protein kinase activity. *Mol. Biol. Cell.* **9**, 2361-2374 (1998).

18. C.J. Bakkenist, and M.B. Kastan, DNA damage activates ATM through intermolecular autophosphorylation and dimer dissociation. *Nature* **421**, 499-506 (2003).

19. A. Dupre, L. Boyer-Catenet, and J. Gautie, Two-step activation of ATM by DNA and the Mre11-Rad50-Nbs1 complex. *Nature Struct. & Mol. Biol*. **13**, 451-457 (2006).

20. E.P. Rogakou, D.R. Pilch, A.H. Orr, V.S. Ivanova, and W.M. Bonner, DNA double-strand breaks induce histone H2AX phosphorylation on serine 139. *J. Biol. Chem*. **273**, 5858-5868 (1998).

21. T.T. Paull, E.P. Rogakou, V. Yamazaki, C.U. Kirchgessner, M. Gellert, and W.M. Bonner, A critical role for histone H2AX in recruitment or repair factors to nuclear foci after DNA damage. *Curr. Biol*., **10**, 886-895 (2000).

22. K. Rothkmann, and M. Lobrich, Evidence for a lack of DNA double-strand break repair in human cells exposed to very low x-ray doses. *Proc. Natl. Acad. Sci. USA* **100**, 5057-5062 (2003).

23. E.L. Leatherbarrow, J.V. Harper, F.A. Cucinotta, and P. O'Neill, Induction and quantification of γ-H2AX foci formation following low- and high-LET radiation. *Int J. Radiat. Biol.* **82**, 111-118 (2006).

24. P.L. Olive, J.P. Banath, Phosphorylation of Histone H2AX as a measure of radiosensitivity. *Int. J. Radiat Oncol*. **58**, 331-335 (2004).

25. J.P. Banath, S.H. MacPhail, and P.L. Olive, Radiation sensitivity, H2AX phosphorylation, and kinetics of repair of DNA strand breaks in irradiated cervical cancer cell lines. *Cancer Res.* **64**, 7144-7149 (2004).

26. L. Alberghina, and H.V. Westerhoff, Systems Biology. Definitions and Perspectives. Topics in Current Genetics, Vol. 13, Springer-Verlag (2005).

27. D.T. Goodhead, Initial events in the cellular effects of ionising radiation: clustered damage in DNA. *Int. J. Radiat. Biol.* **65**, 7-17 (1994).

28. H. Nikjoo, P. O'Neill, W.E. Wilson, and D.T. Goodhead, Computational approach for determining the spectrum of DNA damage induced by ionizing radiation. *Radiat. Res.*, **156**, 577-583 (2001).

29. M. Gulston, J. Fulford, T. Jenner, C. de Lara, and P. O'Neill, Clustered DNA damage induced by γ-radiation in human fibroblasts (HF19), hamster (V79-4) cells and plasmid DNA is revealed as Fpg and Nth sensitive sites. *Nucl. Acids Res*. **30**, 3464-3472 (2002).

30. Ward, I. M. and Chen, J., Histone H2AX is phosphorylated in an ATR-dependent manner in response to replicational stress. *J. Biol. Chem*. **276,** 47759-47762 (2001).

31. S. Jin, and D.T. Weaver, Double-strand break repair by Ku70 requires heterodimerization with Ku80 and DNA binding functions. *The EMBO J*. **16**, 6874-6885 (1997).

32. M. Jovanovic and W.S. Dynan, Terminal DNA structure and ATP influence binding parameters of the DNA-dependent protein kinase at an early step prior to DNA synapsis. *Nucl. Acid Res.* **34**, 1112-1120 (2006).

33. E. Weterings, N. S. Verkaik, H.T. Bruggernwirth, J.H.J. Hoejimakers, and D.C. van Gent, The role of DNA dependent protein kinase in synapsis of DNA ends. *Nucl. Acids Res*. **31**, 7238-7246 (2003).

34. T. Stiff, M. O'Driscoll, N. Rief, K. Iwabuhi, M. Lobrich, and P.A. Jeggo, ATM and DNA-PK function redundantly to phosphorylate H2AX after exposure to ionizing radiation. *Cancer Res.* **64**, 2390-2396 (2004).

35. P.O. Mari, et al. Dynamic assembly of end-joining complexes requires interaction between Ku70/80 and XRCC4. *Proc. Natl. Acad. Sci. U.S.A.* **103**, 18597-18602 (2006).

36. Y.V.R. Reddy, Q. Ding, S.P. Lee-Miller, K. Meek, and D.A. Ramsden, Non-homologous end joining requires that the DNA-PK complex undergo an autophosphorylation-dependent rearrangement at DNA ends. *J. Biol. Chem.* **279**, 39408-39413 (2004).

37. W.D. Bloch, Y. Yu, D. Merkle, J.L., Gifford, Q. Ding, K. Meek, and S.P. Lees-Miller, Autophosphorylation-dependent remodeling of the DNA-dependent protein kinase catalytic subunit regulated ligation of DNA ends. *Nucl. Acids. Res.* **32**, 4351-4357 (2004).

38. B. Rydberg, Radiation-induced heat-labile sites that convert into DNA double-strand breaks. *Radiat. Res.* **153**, 805-12 (2000).

39. B. Sternerlow, K.H. Karlsson, B. Cooper, and B. Rydberg, Measurement of prompt DNA double-strand breaks in mammalian cells without inducing heat-labile sites: results for cells deficient in nonhomologous end joining. *Radiat. Res.* **159**, 502-510 (2003).

40. T.T. Paull, and M. Gilbert, The 3' to 5' exonuclease activity of Mre11 facilitates repair of DNA double-strand breaks. *Mol. Cell.* **1**, 869-879 (1998).

41. C. von Kobbe et al., Werner syndrome protein contains three structure-specific DNA binding domains. *J. Biol. Chem.* **278**, 52997-53006 (2003).

42. S.C. Short, S. Bourne, C. Martindale, M. Woodcock, and S.P. Jackson, DNA damage responses to low radiation doses. *Radiat. Res.* **164**, 292-302 (2005).

43. National Academy of Sciences Committee on Biological Effects of Ionizing Radiation, Health risks from exposure to low levels of ionizing radiation. BEIR VII National Academy Press, Washington D.C. (2005).

44. F.A. Cucinotta, and M. Durante, Cancer risk from exposure to galactic cosmic rays: implications for space exploration by human beings. *The Lancet Oncology* **7**, 431-435, (2006).

45. A. Ponomarev, and F.A. Cucinotta, Chromatin loops are responsible for higher counts of small DNA fragments induced by high-LET radiation, while chromosomal domains do not affect the fragment sizes. *Inter. J. Radiat. Biol.* **82**, 293-305, (2006).

Table 1. Values of Rate-constants and other parameters in the Biochemical Model [a),b)].

Rate Constant	*V79 Cells*	*HF19 cells*	*T98G*
α, Gy^{-1}	16	25	25
$\kappa_{3,}$ hr^{-1}	8 (0.5)	8 (0.5)	8 (0.5)
$k_{P1,}$ hr^{-1}	10	10	10
$k_{P2,}$ hr^{-1}	10 (0.5)	10 (0.5)	10 (0.5)
$\kappa_{P\gamma,}$ $copy^{-1}$ hr^{-1}	1000	900	1000
k_{Dc}, hr^{-1}	4	4	2
$k_{D\gamma,}$ hr^{-1}	2	2	0.75
κ_M	0.5	0.5	0.5
k_{res}, hr^{-1}	0 (0.05)	0 (0.05)	0 (0.05)

a) Values of κ_1 , κ_2, and H_1 are set at 100 hr^{-1}, 100 hr^{-1}, and 3000 per cell for all cell lineages considered. Values chosen correspond to a peak for a DSB-$Ku_{70/80}$ complex at about 1 min post-irradiation (35), and assuming peak of DSB-$Ku_{70/80}$-DNA-PK_{cs} complex at about 3 min post-irradiation.

b) The initial number of breaks per Gy (α) determined from experiments of Gulston *et al.* (34). We use the same values for GM5738 cells as HF19.

Figure Captions:

Fig. 1. Schematic of biochemical kinetics model of DSB repair by NHEJ with induction of γH2AX by DNA-PK_{cs}. The key components of the model and associated rate-constants are show. Not illustrated is the degradation of the $[C_3]$ complex after the ligation step nor distinction between simple and complex DSB including the formation of residual DSB when complex initial DSB do not proceed to the $[C_2^{PP}]$ complex.

Fig. 2. Model calculations of time course for sequence of DNA repair complexes in NHEJ pathway, and DSB rejoining curve (non-complex only) for 1-Gy gamma-ray exposures in normal human diploid fibroblast cells.

Fig. 3. Model calculations for the time-course of Ku70/80 hetero-dimers in complex with DSB and other NHEJ components compared to live cell imaging data from ref. (35) for EGFP-Ku_{80} induction after irradiation of CHO cells with a near infrared laser.

Fig. 4. Comparisons of model calculations to DSB rejoining determined by PFGE method for GM5758 (human diploid fibroblast cells) at 40 Gy (37). The solid line shows the contributions from simple and complex DSB. For comparison we show calculations of the rejoining curves for simple and complex DSB in our model normalize to unity as dash and dotted lines, respectively.

Fig. 5. Comparisons of model calculations to measurements of γH2AX foci by Leatherbarrow *et al*. (23) with solid line for total (simple and complex DSB) induced γH2AX foci, dash line foci from simple DSB alone, and dotted line the number of DSB remaining. Symbols with error bars are the experimental results (23).

a) HF19 Cells at 1 Gy
b) V79 Cells at 1 Gy

Fig. 6. Comparisons of model calculations for dose-response for γH2AX foci at 0.5 (closed circles) and 4 hrs (open triangles) post-irradiation data of Short *et al.* (34). Model calculations shown are solid line at 0.5 hr, dash line at 4 hr post-irradiation.

Fig. 7. Predictions for the number of DSB repair complexes versus dose for various dose-rates in human fibroblast cells.

Fig. 1

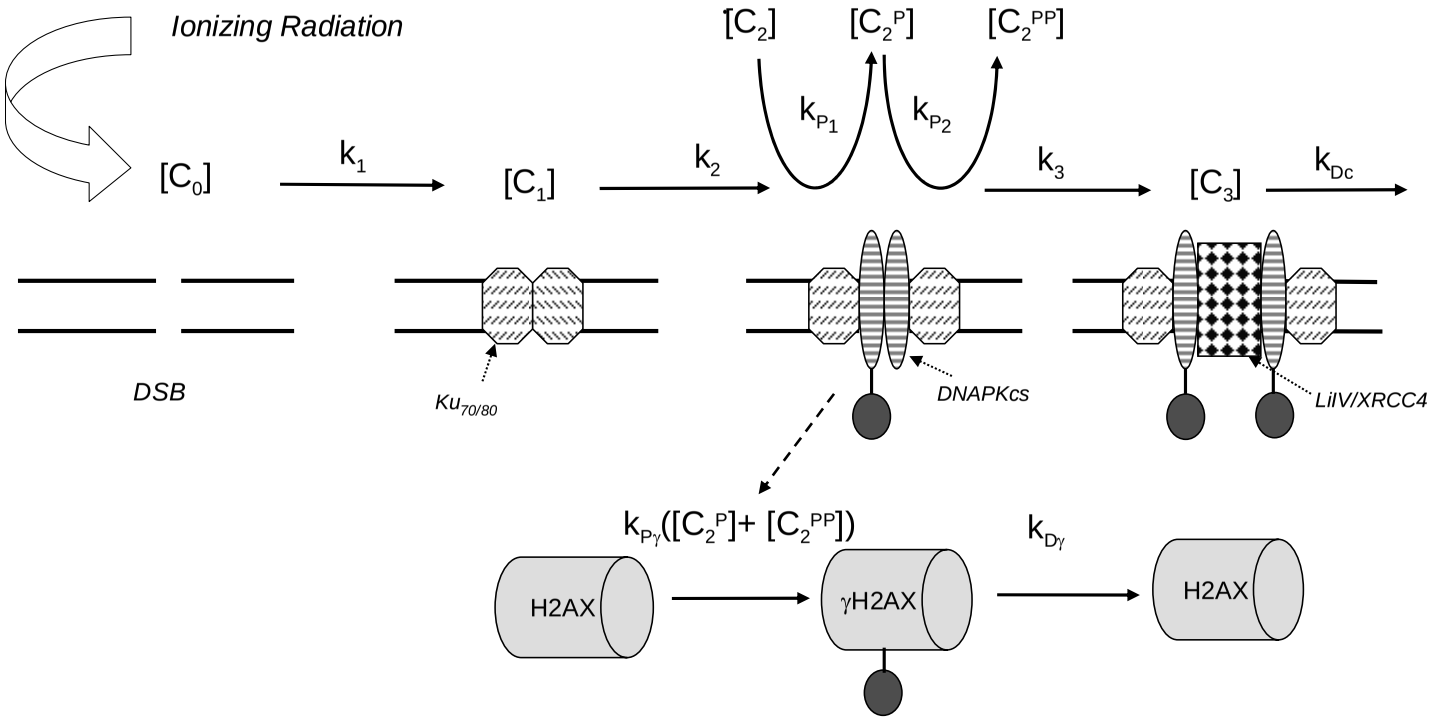
Ionizing Radiation
[C0]
k1
[C1]
k2
[C2]
[C2P]
[C2PP]
kP1
kP2
k3
[C3]
kDc
DSB
Ku70/80
DNAPKcs
LilV/XRCC4
kPγ([C2P]+ [C2PP])
kDγ
H2AX
γH2AX
H2AX

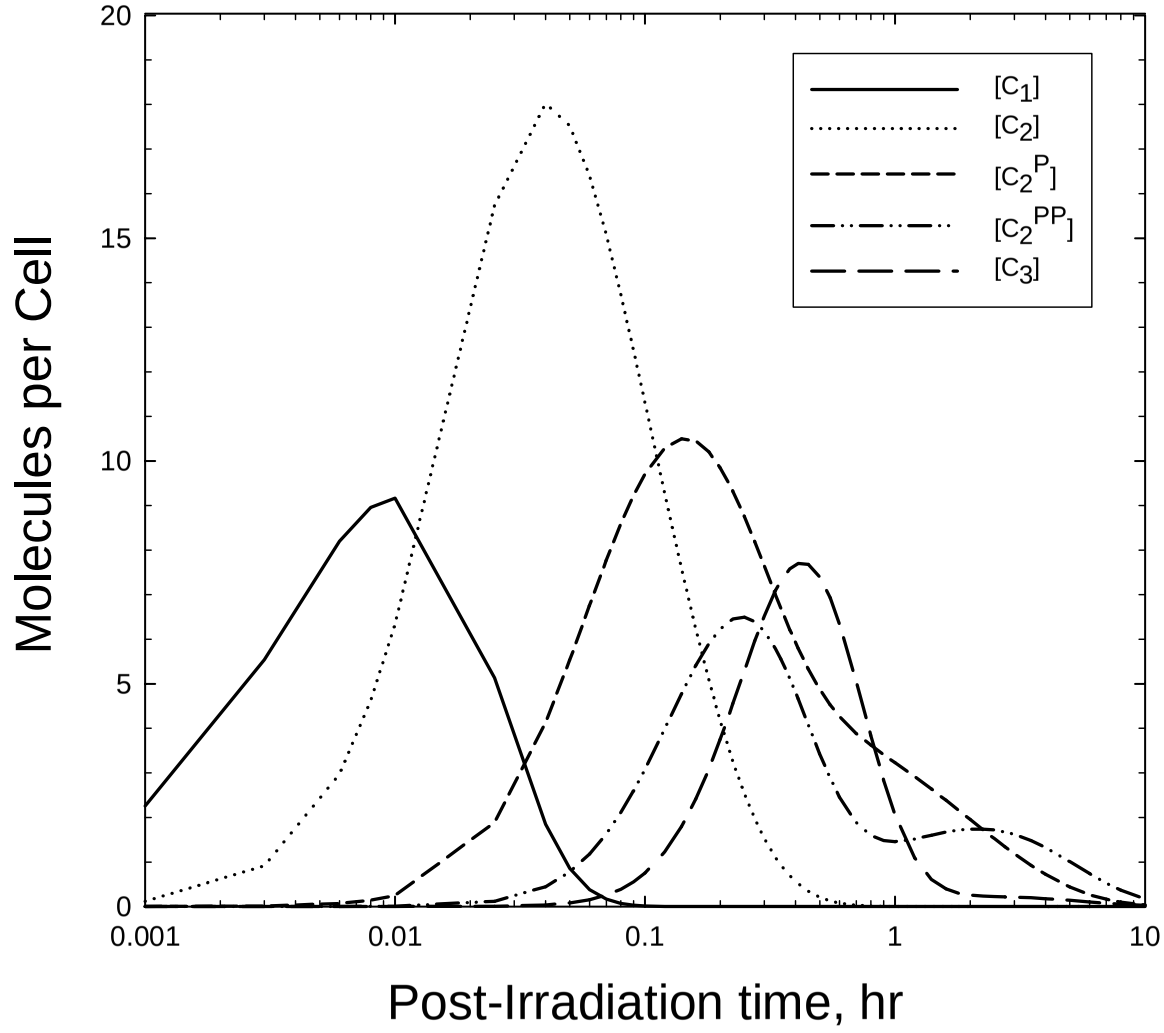
20
15
10
5
0
0.001
0.01
0.1
1
10
Molecules per Cell
Post-Irradiation time, hr
[C1]
[C2]
[C2P]
[C2PP]
[C3]

Fig. 2.

Fig. 3.

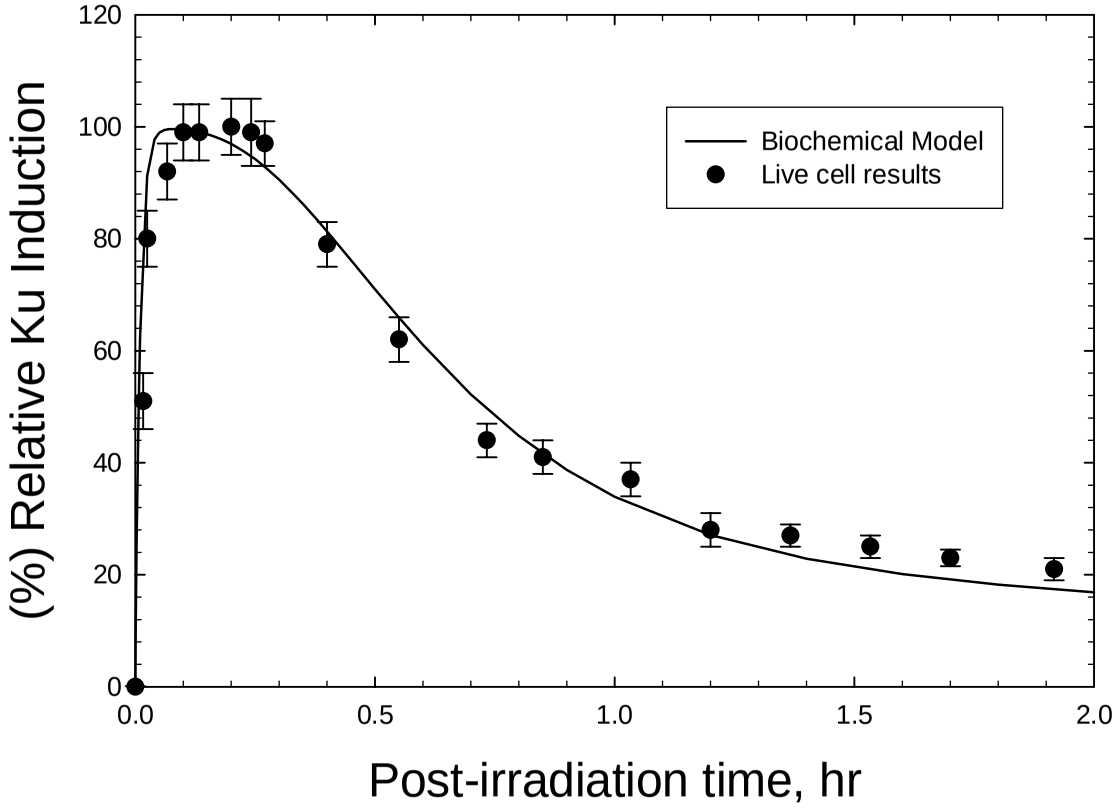
(%) Relative Ku Induction
Post-irradiation time, hr
Biochemical Model
Live cell results
0
20
40
60
80
100
120
0.0
0.5
1.0
1.5
2.0

Fig. 4

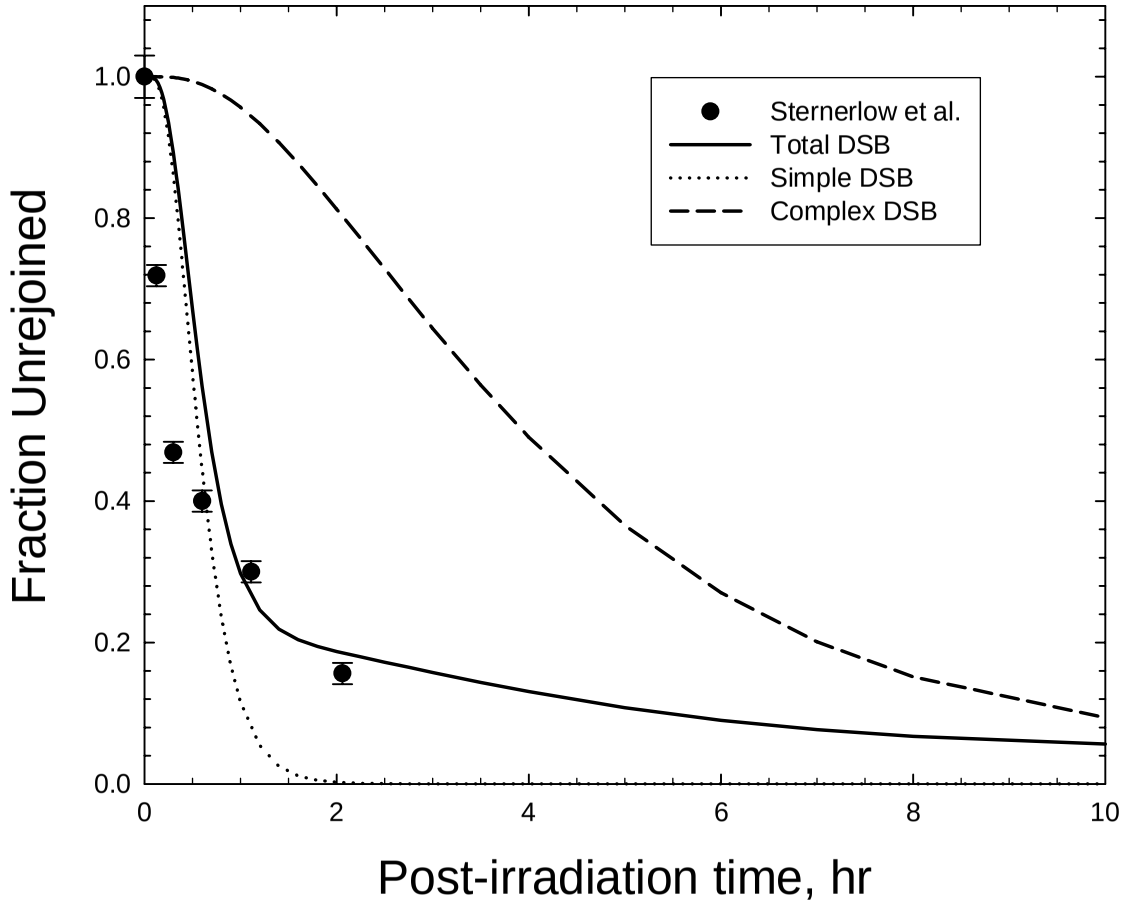
Fraction Unrejoined
Post-irradiation time, hr
Sternerlow et al.
Total DSB
Simple DSB
Complex DSB
1.0
0.8
0.6
0.4
0.2
0.0
0
2
4
6
8
10

Fig. 5a.

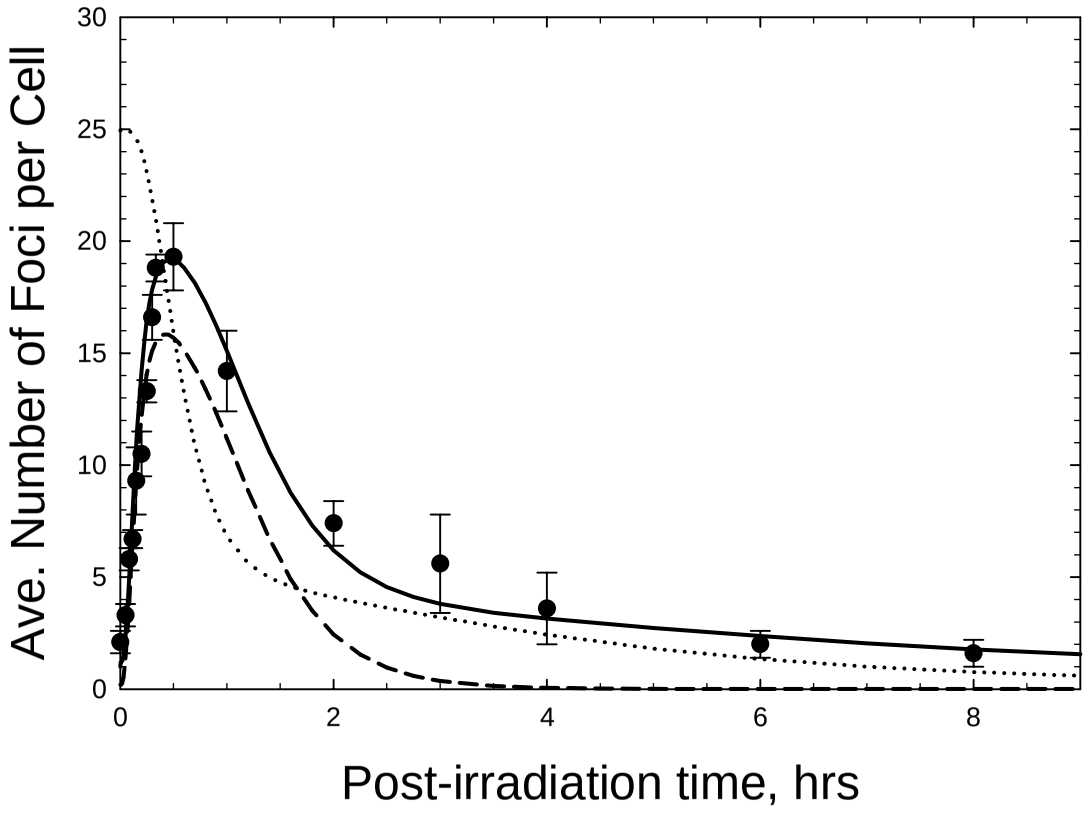
Ave. Number of Foci per Cell
Post-irradiation time, hrs
0
5
10
15
20
25
30
0
2
4
6
8

Fig. 5b.

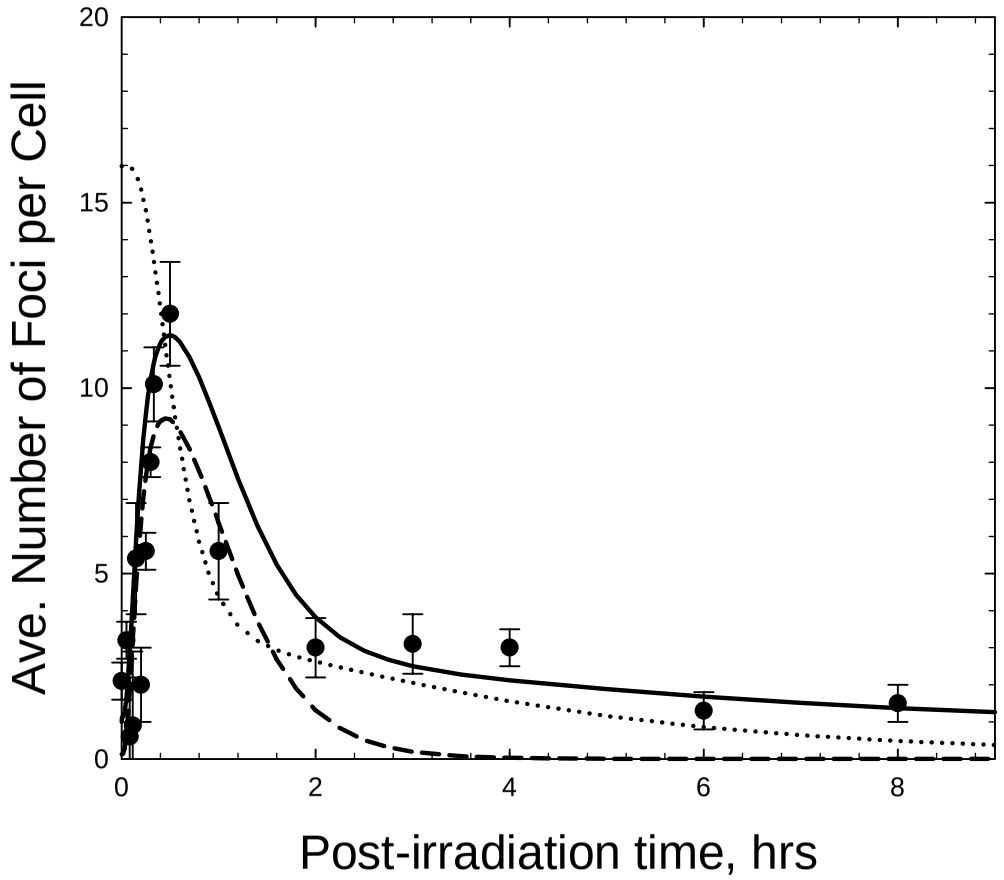
Ave. Number of Foci per Cell
Post-irradiation time, hrs
0
5
10
15
20
0
2
4
6
8

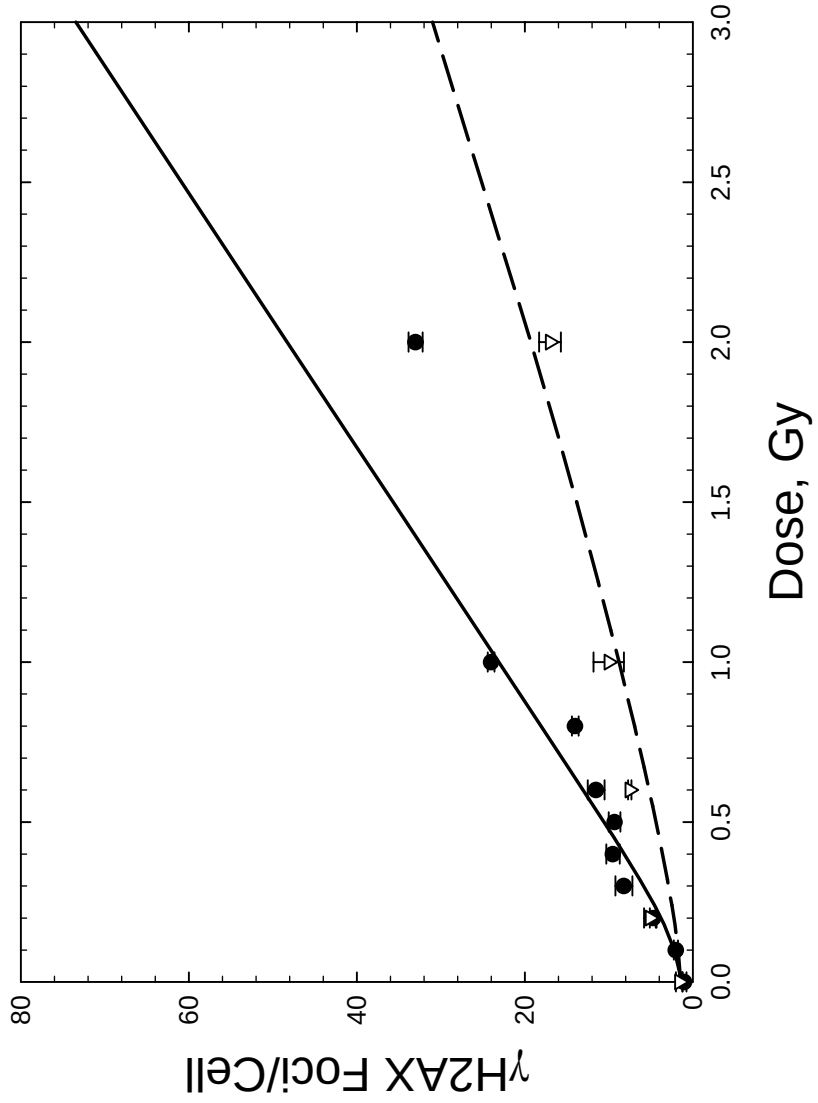

Fig. 6.

Fig. 7